

# A High Order Discontinuous Galerkin Method for Fluid-Structure Interaction

Per-Olof Persson\* and Jaime Peraire†

*Massachusetts Institute of Technology, Cambridge, MA 02139, U.S.A.*

Javier Bonet‡

*University of Wales Swansea, Swansea SA2 8PP, U.K.*

We describe a method for computing time-dependent solutions to the compressible Navier-Stokes equations coupled to a hyperelastic Neo-Hookean membrane model. The deforming domain is handled by introducing a continuous mapping between a fixed reference configuration and the time varying domain, and rewriting the Navier-Stokes equations as a conservation law for the independent variables in the reference configuration. The spatial discretization is carried out using the Discontinuous Galerkin method on unstructured meshes of triangles, and the membrane model is discretized with regular finite elements. The method uses an explicit smooth mapping for the entire domain which is differentiated to obtain accurate grid velocities and deformation gradients. This mapping is constructed by a combination of spline interpolation and high order blending functions. Various examples are shown to illustrate the methods, and elastic and rigid membranes are compared.

## I. Introduction

There is a growing interest in high order methods for fluid problems, largely because of their ability to produce highly accurate solutions with minimum numerical dispersion. The Discontinuous Galerkin (DG) method produces stable discretizations of the convective operator for any order discretization. Moreover, it can be used with unstructured meshes of simplices, which appears to be a requirement for real-world complex geometries. In this paper, we present a high order DG formulation for the Navier-Stokes equations coupled to a finite element model of a non-linear membrane.

Many approaches have been suggested for the simulation of fluid-structure interaction,<sup>1-3</sup> and a common way to treat the deformable domains is the use of Arbitrary Lagrangian Eulerian (ALE) methods.<sup>4-7</sup> In these efforts the discretization on the deformable domain is carried out on a deforming grid and thus the metric changes over time. Only second (or at most third) order accuracy for space and time have been demonstrated.<sup>8</sup>

Here, we use the approach that we presented in Ref. 9. Inspired by techniques used with finite difference methods,<sup>10</sup> we construct a time varying mapping between a fixed reference domain and the real time-varying domain geometry. The actual computation is carried out on a fixed mesh and the variable domain geometry is accounted for through a modification of the fluxes in the conservation law. This approach is simple and allows for arbitrarily high order solutions to be obtained. To satisfy the Geometric Conservation Law, we solve an additional scalar equation that compensates for integration errors.

For the non-linear membrane model we use a continuous Galerkin discretization, integrated in time simultaneously with the DG discretization. The forces from the fluid are applied to the membrane, and the membrane displacements provide the deformation of the fluid domain. We note that this monolithic treatment provides a time-accurate coupling, unlike other approaches where the fluid and the structure are integrated separately, and forces and displacements are only transferred at the end of each timestep. We do

---

\*Instructor, Department of Mathematics, MIT, 77 Massachusetts Avenue 2-363A, Cambridge, MA 02139. E-mail: persson@mit.edu. AIAA Member.

†Professor, Department of Aeronautics and Astronautics, MIT, 77 Massachusetts Avenue 37-451, Cambridge, MA 02139. E-mail: peraire@mit.edu. AIAA Associate Fellow.

‡Professor, School of Engineering, University of Wales Swansea, Swansea SA2 8PP, U.K. E-mail: j.bonet@swansea.ac.uk.

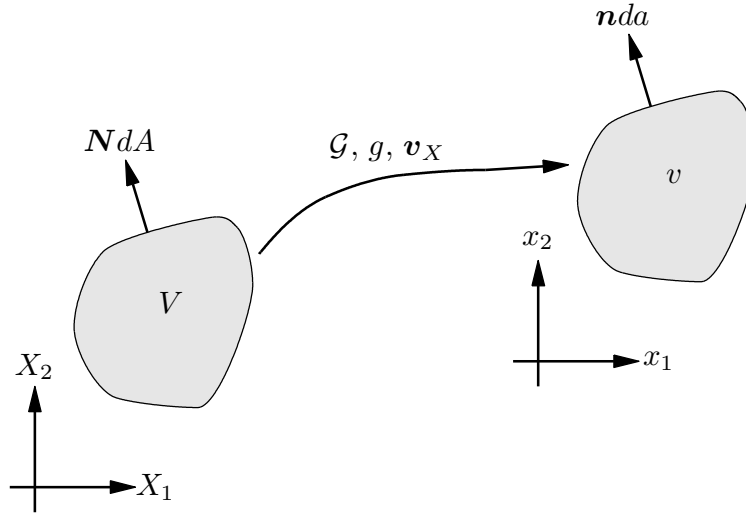


Figure 1. Mapping between the physical and the reference domains.

not explicitly enforce consistent loads at the interface,<sup>11</sup> but rely on the high order formulation to produce accurate results.

We show examples that compare elastic and rigid membranes and observe that in some cases the elastic membrane has better aerodynamical properties due to its ability to deform and better align with the flow.

## II. Governing Equations

### A. The ALE Formulation for Navier-Stokes Equations

When simulating problems involving time varying domains, the motion of the mesh must be accounted for in the solution process. An important ingredient for our formulation is a time dependent mapping between a fixed reference domain and the physical deformable domain. Let the physical domain of interest be denoted by  $v(t)$  and the fixed reference configuration be denoted by  $V$  (see figure 1). Let  $\mathcal{G}(\mathbf{X}, t)$  denote a one-to-one time dependent mapping between  $V$  and  $v(t)$ . Thus a point  $\mathbf{X}$  in  $V$ , is mapped to a point  $\mathbf{x}(t)$  in  $v(t)$ , which is given by  $\mathbf{x} = \mathcal{G}(\mathbf{X}, t)$ . We introduce the mapping deformation gradient  $\mathbf{G}$  and the mapping velocity  $\mathbf{v}_X$  as

$$\mathbf{G} = \nabla_{\mathbf{X}} \mathcal{G}, \quad \mathbf{v}_X = \left. \frac{\partial \mathcal{G}}{\partial t} \right|_{\mathbf{X}}. \quad (1)$$

In addition, we denote the Jacobian of the mapping by  $g = \det(\mathbf{G})$ . We can then re-write the Navier-Stokes equations in the physical domain  $(\mathbf{x}, t)$ ,

$$\left. \frac{\partial \mathbf{U}_x}{\partial t} \right|_{\mathbf{x}} + \nabla_{\mathbf{x}} \cdot \mathbf{F}_x(\mathbf{U}_x, \nabla_{\mathbf{x}} \mathbf{U}_x) = 0, \quad (2)$$

as an equivalent local conservation law in the reference domain:

$$\left. \frac{\partial \mathbf{U}_X}{\partial t} \right|_{\mathbf{X}} + \nabla_{\mathbf{X}} \cdot \mathbf{F}_X(\mathbf{U}_X, \nabla_{\mathbf{X}} \mathbf{U}_X) = 0, \quad (3)$$

where the transformed vector of conserved quantities, its derivatives, and the corresponding fluxes in the reference space are:

$$\mathbf{U}_X = g \mathbf{U}_x, \quad (4)$$

$$\nabla_{\mathbf{x}} \mathbf{U}_x = \nabla_{\mathbf{X}} (g^{-1} \mathbf{U}_X) \mathbf{G}^{-T} = (g^{-1} \nabla_{\mathbf{X}} \mathbf{U}_X - \mathbf{U}_X \nabla_{\mathbf{X}} (g^{-1})) \mathbf{G}^{-T}, \quad (5)$$

$$\mathbf{F}_X = g \mathbf{G}^{-1} \mathbf{F}_x - \mathbf{U}_X \mathbf{G}^{-1} \mathbf{v}_X. \quad (6)$$

We refer to Ref. 9 for details on the derivation of this transformation.

## B. Non-linear Membrane Model

For the structural part of our simulations, we use a hyperelastic Neo-Hookean membrane formulation with viscous, fluid like, dissipation.<sup>12</sup> The membrane position is given by a mapping  $\mathbf{x} = \phi(X, t)$ , where the unstretched reference configuration corresponds to  $\mathbf{x}_0 = \phi(X, 0)$ . From this we can compute the mapping velocity and the deformation gradients by

$$\mathbf{v} = \frac{\partial \phi}{\partial t}, \quad F = \frac{\partial \phi}{\partial X}(X, t), \quad F_0 = \frac{\partial \phi}{\partial X}(X, 0). \quad (7)$$

From this we can calculate the Cauchy-Green stress as

$$C = F^T F, \quad C_0 = F_0^T F_0. \quad (8)$$

The governing equations for the membrane are then given by

$$\begin{aligned} \frac{\partial \bar{\rho}_0 \mathbf{v}}{\partial t} &= \frac{\partial P}{\partial X} + P_X, \\ \frac{\partial \mathbf{x}}{\partial t} &= \mathbf{v}, \end{aligned} \quad (9)$$

where  $P_X$  is the external force per unit reference area,  $\bar{\rho}_0 = \rho_0 H \sqrt{C_0}$  is the mass per unit reference area, and  $H$  is the thickness. Note that although the system (9) can be written in terms of  $\mathbf{x}$  only, we choose this form to be able to couple with the flow. The first Piola-Kirchoff stress is  $P = F(S + S_v)$  where  $S$  is the second Piola-Kirchoff stress which is derived from the strain energy potential  $\psi(C, C_0)$  as

$$S = 2 \frac{\partial \psi(C, C_0)}{\partial C}. \quad (10)$$

For a Neo-Hookean material,

$$\psi(C, C_0) = \frac{1}{2} \mu H \sqrt{C_0} \left( \frac{C}{C_0} + \frac{C_0}{C} - 3 \right). \quad (11)$$

Finally, the viscous stresses  $S_v$  are written as

$$S_v = 4\nu H \frac{\sqrt{C_0}}{C^2} \left( F^T \frac{\partial \mathbf{v}}{\partial X} \right). \quad (12)$$

## III. Numerical Methods

### A. Numerical Discretization

In order to develop a DG method, we rewrite the above problem (3) as a system of first order equations

$$\frac{\partial \mathbf{U}_X}{\partial t} + \nabla_X \cdot \mathbf{F}_X(\mathbf{U}_X, \mathbf{Q}_X) = 0 \quad (13)$$

$$\mathbf{Q} - \nabla_X \mathbf{U}_X = 0. \quad (14)$$

Next, we introduce the 'broken' DG spaces  $\mathcal{V}^h$  and  $\Sigma^h$  associated with the triangulation  $\mathcal{T}^h = \{K\}$  of  $V$ . In particular,  $\mathcal{V}^h$  and  $\Sigma^h$  denote the spaces of functions whose restriction to each element  $K$  are polynomials of order  $p \geq 1$ .

Following Ref. 13, we consider DG formulations of the form: find  $\mathbf{U}_X^h \in \mathcal{V}^h$  and  $\mathbf{Q}_X^h \in \Sigma^h$  such that for all  $K \in \mathcal{T}^h$ , we have

$$\int_K \frac{\partial \mathbf{U}_X^h}{\partial t} \mathbf{V} \, dV - \int_K \mathbf{F}_X(\mathbf{U}_X^h, \mathbf{Q}^h - X) \cdot \nabla_X \mathbf{V} \, dV - \int_{\partial K} \mathbf{V}(\hat{\mathbf{F}}_X \cdot \mathbf{N}) \, dA = 0, \quad \forall \mathbf{V} \in \mathcal{V}^h, \quad (15)$$

$$\int_K \mathbf{Q}_X^h \mathbf{P} \, dV + \int_K \mathbf{U}_X^h \nabla_X \cdot \mathbf{V} \, dV - \int_{\partial K} \hat{\mathbf{U}}_X^h(\mathbf{P} \cdot \mathbf{N}) \, dA = 0, \quad \forall \mathbf{P} \in \Sigma^h. \quad (16)$$

Here, the numerical fluxes  $\hat{\mathbf{F}}_X \cdot \mathbf{N}$  and  $\hat{\mathbf{U}}_X$  are approximations to  $\mathbf{F}_X \cdot \mathbf{N}$  and to  $\mathbf{U}_X$ , respectively, on the boundary of the element  $K$ . The DG formulation is complete once we specify the numerical fluxes  $\hat{\mathbf{F}}_X \cdot \mathbf{N}$  and  $\hat{\mathbf{U}}_X$  in terms of  $(\mathbf{U}_X^h)$  and  $(\mathbf{Q}_X^h)$  and the boundary conditions. The flux term  $\hat{\mathbf{F}}_X \cdot \mathbf{N}$  is decomposed into its inviscid and viscous parts. The numerical fluxes for the viscous terms are chosen according to the Compact Discontinuous Galerkin (CDG) method,<sup>14</sup> and the inviscid numerical flux  $\hat{\mathbf{F}}_N^{\text{inv}}(\mathbf{U}_X^h)$  is chosen according to the method proposed by Roe.<sup>15</sup> This flux can be very easily derived from the standard Eulerian Roe fluxes, see Ref. 9 for details.

The membrane equation (9) is discretized in space using a piecewise linear continuous finite element method, see Ref. 12 for details. The source terms are obtained by numerical integration of the forces  $P_X$  from the fluid. Time integration is performed explicitly using a fourth-order Runge-Kutta scheme. The fluid and the structure are integrated in time simultaneously, with the forces from the fluid and the displacements of the membrane being treated as fully continuous functions in time. This results in a time-accurate coupling at the interface. Note that the computation of the interaction terms is simplified by our mapping approach, since the forces are defined in the fixed reference domains.

## B. Geometric Conservation Law

It turns out that, for arbitrary mappings, a constant solution in the physical domain is not necessarily a solution of the discretized equations in the reference domain. Even though this error is typically very small for high order discretizations, the situation is quite severe for lower order approximations since the free-stream condition is not preserved identically. Satisfaction of the constant solution is often referred to as the Geometric Conservation Law (GCL) and is was originally discussed in Ref. 16. The source of the problem is the inexact integration of the Jacobian  $g$  of the transformation by the numerical scheme.

Here, we use the approach that we presented in Ref. 9 to satisfy the GCL. The system of conservation laws (3) is replaced by

$$\left. \frac{\partial(\bar{g}g^{-1}\mathbf{U}_X)}{\partial t} \right|_X - \nabla_X \cdot \mathbf{F}_X = \mathbf{0}, \quad (17)$$

where  $\bar{g}$  is obtained by solving the following equation using the same numerical scheme

$$\left. \frac{\partial \bar{g}}{\partial t} \right|_X - \nabla_X \cdot (g\mathbf{G}^{-1}\mathbf{v}_X) = 0. \quad (18)$$

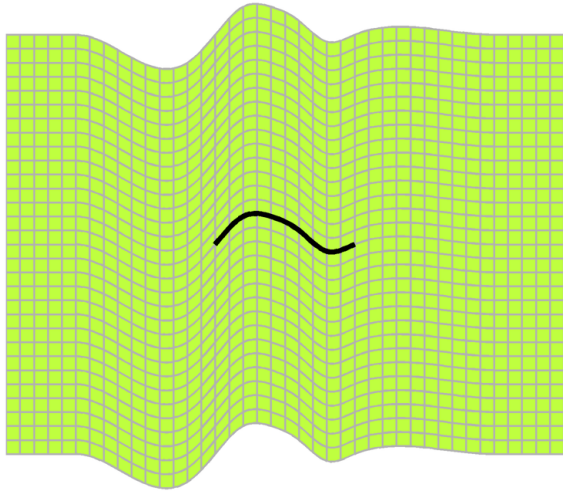
We note that even though  $\bar{g}$  is an approximation to  $g$ , when the above equation is solved numerically its value will differ from that of  $g$  due to integration errors. It is straightforward to verify that (17) does indeed preserve a constant solution as desired. Finally, we point out that since the fluxes in equation (18) are continuous, the numerical flux is trivial to compute. Moreover, we note that equation (18) does not require information from neighboring elements and therefore can be solved on each element independently.

## C. Explicit Mappings for Deforming Membrane

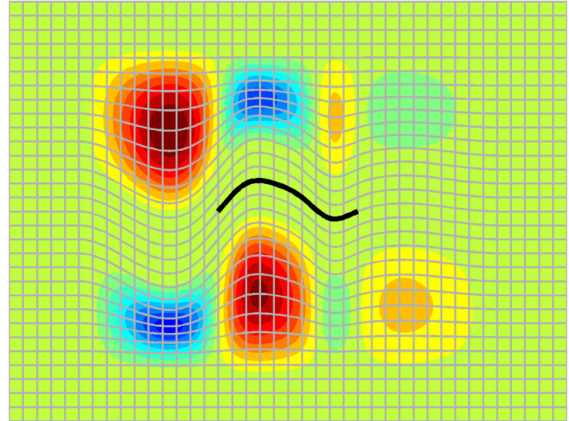
In order to solve problems on moving domains, we need a procedure to define a mapping  $\mathbf{x} = \mathcal{G}(\mathbf{X}, t)$  from the reference domain to the physical domain. One method that is commonly used in ALE simulations is to force the motion of the mesh nodes on the boundary and apply a mesh smoothing scheme to reconstruct the mapping in the domain interior. Another technique is to solve additional equations (usually elliptic) for  $\mathbf{x}$  in the interior. For some of these algorithms, it may not be obvious to obtain accurate values for the mapping derivatives as required by our fluxes.

In this example we use a different approach which produces explicit expressions for the mappings, similar to the blending method for rigid deformations that we presented in Ref. 9. The goal is to produce a mapping in the entire domain that deforms the membrane according to a given shape, reduces to the identity mapping away from the membrane, and is smooth in-between. To do this we use polynomial *blending functions*  $r_n(x)$  of odd degree  $n$ , with  $r(0) = 0$ ,  $r(1) = 1$ , and with  $(n-1)/2$  vanishing derivatives at  $x = 0$  and  $x = 1$ . For degree  $n = 3$  this blending polynomial equals  $r_3(x) = 3x^2 - 2x^3$ , and for  $n = 5$  it equals  $r_5(x) = 10x^3 - 15x^4 + 6x^5$ . For convenience we also define  $r_n(x) = 0$  when  $x < 0$  and  $r_n(x) = 1$  when  $x > 1$ .

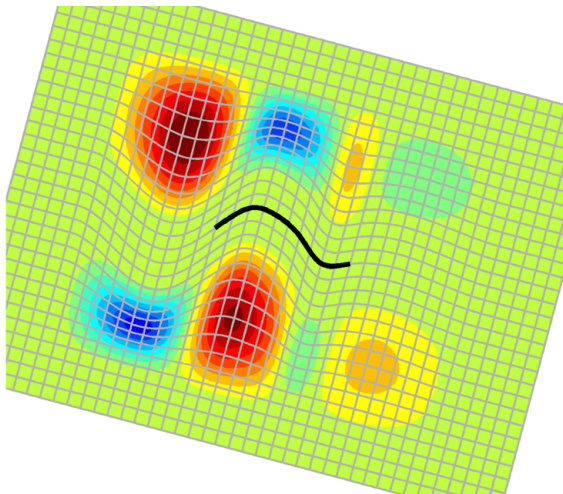
The four steps of our explicit construction are illustrated in figure 2, and details are given below.



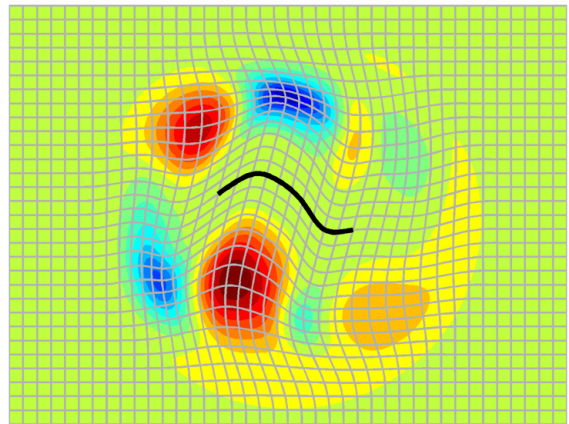
1) Spline mapping



2) Blending in  $|Y|$



3) Rotation/Translation



4) Blending in  $R$

Figure 2. The four steps of the explicit mapping for a deforming membrane. The color shows the determinant of the deformation gradient  $g$ , from low (blue) to high (red).

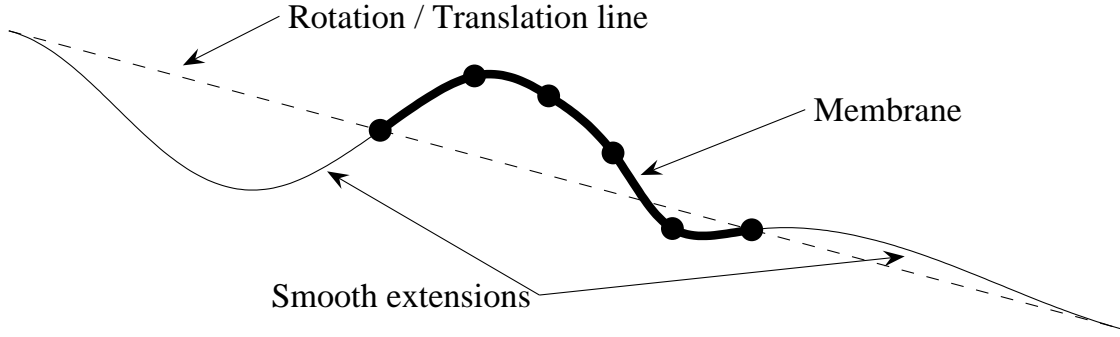


**Figure 3.** Fitting a cubic spline to the membrane points and extending smoothly on each side.

1. First we fit a cubic spline  $y_c(X)$  to the membrane shape, where the  $X$ -axis is the straight line between the membrane endpoints, see figure 3. We create smooth extensions to the spline curve one chord length on each side of the membrane, by mirroring two membrane points and specifying zero derivative condition at the ends. We can then map the entire domain by

$$x_1 = X \quad (19)$$

$$y_1 = Y + y_c(X), \quad (20)$$

that is, we move each point  $X, Y$  vertically by the displacement of the spline at coordinate  $X$ .

2. While the mapping from the step 1 is smooth and deforms the membrane correctly (apart from rotation and translation), it deforms the domain excessively away from the membrane. Therefore, we blend smoothly between the spline deformation and the identity mapping:

$$x_2 = b(Y)x_1 + (1 - b(Y))X = X \quad (21)$$

$$y_2 = b(Y)y_1 + (1 - b(Y))Y = Y + (1 - b(Y))y_c(X), \quad (22)$$

where the blending function  $b(Y) = r_n(|Y|/Y_0)$ .

3. Next we rotate and translate the domain by the angle  $\alpha$  and displacement  $\Delta x, \Delta y$  to account for the fact that our spline was computed with respect to the line between the membrane endpoints:

$$x_3 = \Delta x + x_2 \cos \alpha + y_2 \sin \alpha \quad (23)$$

$$y_3 = \Delta y - x_2 \sin \alpha + y_2 \cos \alpha. \quad (24)$$

This will put the spline in its actual position, although the entire domain can be highly deformed.

4. Finally, we blend smoothly between our mapping and the identity mapping, based on the distance  $R = \sqrt{(X - X_{\text{mid}})^2 + (Y - Y_{\text{mid}})^2}$  from the membrane midpoint  $(X_{\text{mid}}, Y_{\text{mid}})$ :

$$x_4 = b(R)x_3 + (1 - b(R))X \quad (25)$$

$$y_4 = b(R)y_3 + (1 - b(R))Y. \quad (26)$$

with blending function  $b(R) = r_n((R - R_0)/(R_1 - R_0))$  for appropriate parameters  $R_0, R_1$ .

The advantage with our explicit mapping is that its derivatives are easily obtainable, either by direct differentiation of each step or numerical differencing. It is clear that the regularity of the mapping must play an important role in the overall accuracy of the scheme. Here, we use quintic  $r_5(x)$  polynomials in all our simulations.

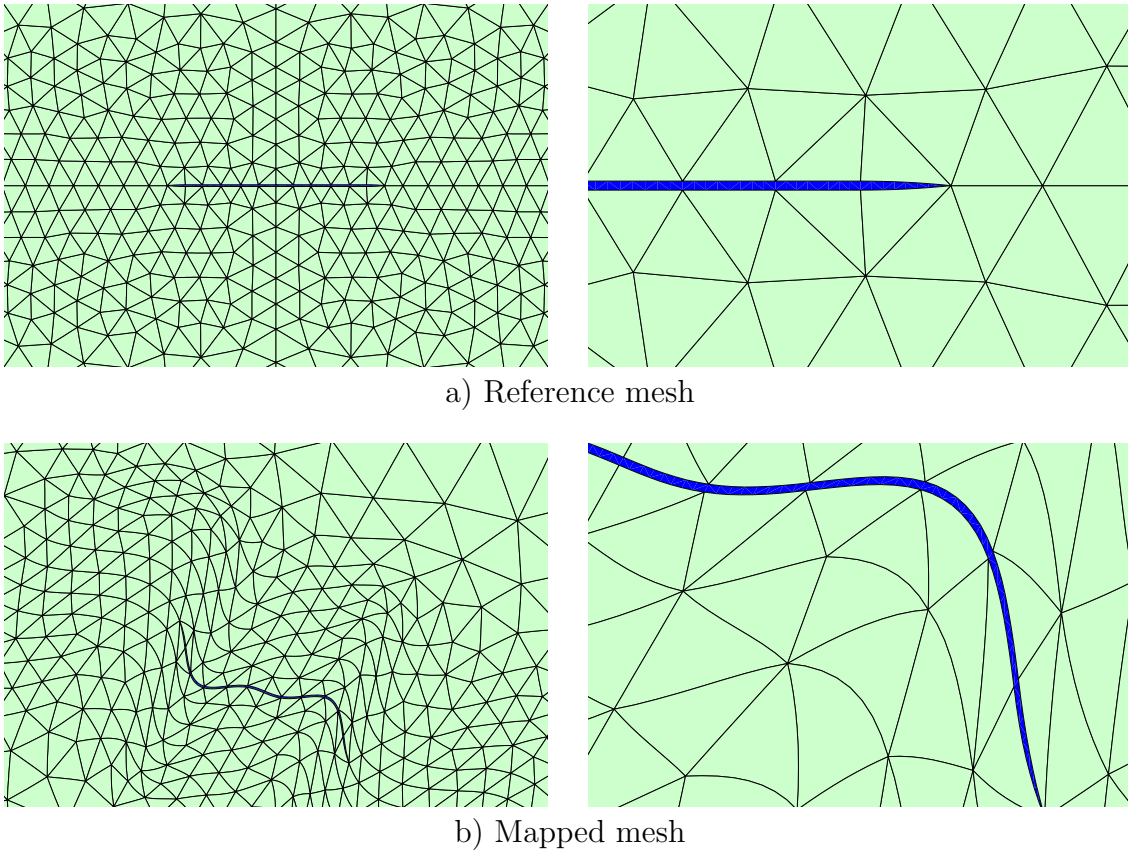


**Figure 4.** The mesh used in the simulation, with polynomial order  $p = 4$  within each triangle. Note that the mapped mesh is in general curved, since the mapping is non-linear in  $X$ .

## IV. Results

We consider the flow around a membrane with fixed endpoints, where the angle  $\alpha$  between the two membrane endpoints are 5, 10, 15, and 20, respectively. The actual membrane in the two dimensional domain is a very thin foil of length 1 and thickness 0.005, with a smooth transition towards the leading and trailing edges. The mesh we used is shown in figure 4, and it contains 784 nodes and 1512 elements. With  $p = 4$  order polynomials within each triangle, this gives a total of 22,680 nodes to solve for, or 113,400 degrees of freedom (including the extra equation for the GCL (18)). For the one dimensional membrane model we use 6 elements of uniform size.

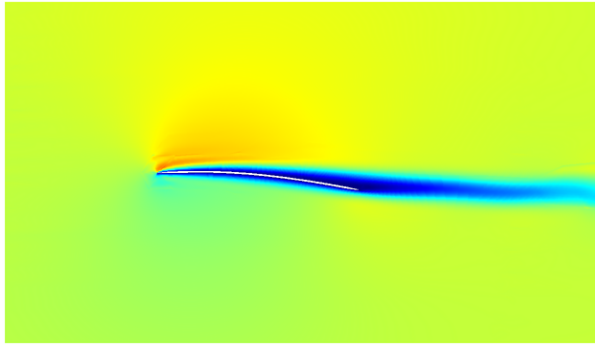
We integrate in time and use both the membrane model (9) and a rigid membrane. The flow properties are  $Re=2000$  and  $Mach=0.2$ , and the elastic membrane properties are  $\rho_0 = 1$ ,  $H = 1$ ,  $\mu = 0.5$ ,  $\nu = 2$ . The unstretched length of the membrane is 40% of the initial length, giving a deformation gradient in the reference configuration of  $F_0 = 0.4$ . Sample solutions are shown in figure 5 for the four angles and the elastic/rigid membranes. The drag and lift forces for all cases are plotted against time in figure 6.

We observe that the flows are almost steady for  $\alpha = 5$ , but highly unsteady for the larger angles. At  $\alpha = 10$  and  $\alpha = 15$  we can see that the elastic membrane aligns with the flow at the leading edge, resulting in smaller vortices and a lower drag force. In all of the cases the elastic membrane is giving a higher average lift force.

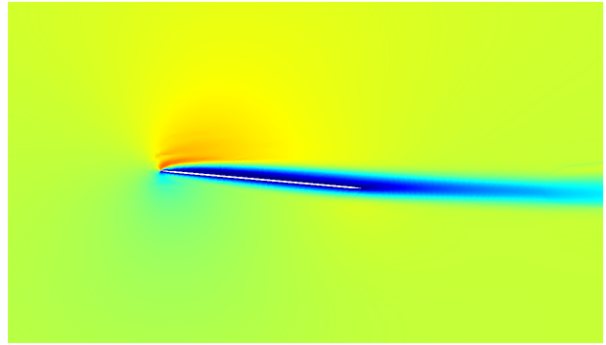
Finally, since our motivation for studying the interaction between fluids and membranes is to asses the impact of membranes on flapping flight,<sup>17</sup> we show a case where the membrane endpoints are oscillating. We specify the location of the left endpoint  $y(t) = A_0 \sin(\omega t)$  with  $A_0 = 0.5$  and  $\omega = 0.2 \cdot 2\pi$ , and the angle to the right endpoint  $\alpha(t) = \alpha_0 \sin(\omega t + \varphi)$  with  $\alpha_0 = 30^\circ$  and  $\varphi = 90^\circ$ . The properties are the same as in the previous case, except for the Reynolds number which is 5000. A sample plot of the Mach number at time  $t = 16.125$  is shown in figure 7, both for the elastic and the rigid membrane.

## References

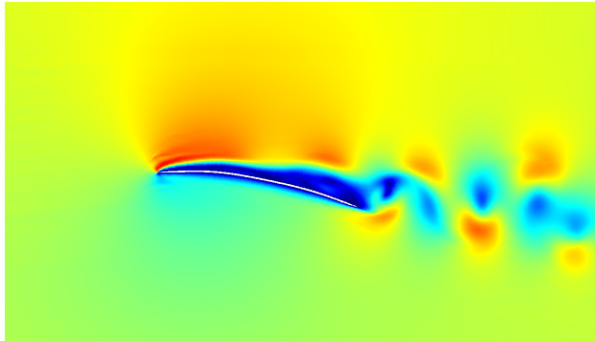
- <sup>1</sup>Yosibash, Z., Kirby, R. M., Myers, K., Szabó, B., and Karniadakis, G., “High-Order Finite Elements for Fluid-Structure Interaction Problems,” *44th AIAA/ASME/ASCE/AHS Structures, Structural Dynamics, and Materials Conference, Norfolk, Virginia*, April 2003, AIAA-2003-1729.
- <sup>2</sup>Reuther, J. J., Alonso, J. J., Martins, J. R. R. A., and Smith, S. C., “A Coupled Aero-Structural Optimization Method For Complete Aircraft Configurations,” *37th AIAA Aerospace Sciences Meeting and Exhibit, Reno, Nevada*, January 1999, AIAA-99-0187.
- <sup>3</sup>Geuzaine, P., Grandmont, C., and Farhat, C., “Design and analysis of ALE schemes with provable second-order time-accuracy for inviscid and viscous flow simulations,” *J. Comput. Phys.*, Vol. 191, No. 1, 2003, pp. 206–227.
- <sup>4</sup>Farhat, C. and Geuzaine, P., “Design and analysis of robust ALE time-integrators for the solution of unsteady flow problems on moving grids,” *Comput. Methods Appl. Mech. Engrg.*, Vol. 193, No. 39-41, 2004, pp. 4073–4095.
- <sup>5</sup>Venkatasubban, C. S., “A new finite element formulation for ALE (arbitrary Lagrangian Eulerian) compressible fluid mechanics,” *Internat. J. Engrg. Sci.*, Vol. 33, No. 12, 1995, pp. 1743–1762.
- <sup>6</sup>Lomtev, I., Kirby, R. M., and Karniadakis, G. E., “A discontinuous Galerkin ALE method for compressible viscous flows in moving domains,” *J. Comput. Phys.*, Vol. 155, No. 1, 1999, pp. 128–159.
- <sup>7</sup>Ahn, H. and Kallinderis, Y., “Strongly coupled flow/structure interactions with a geometrically conservative ALE scheme on general hybrid meshes,” *Journal of Computational Physics*, to appear.
- <sup>8</sup>Formaggia, L. and Nobile, F., “Stability analysis of second-order time accurate schemes for ALE-FEM,” *Comput. Methods Appl. Mech. Engrg.*, Vol. 193, No. 39-41, 2004, pp. 4097–4116.
- <sup>9</sup>Persson, P.-O., Peraire, J., and Bonet, J., “Discontinuous Galerkin Solution of the Navier-Stokes Equations on Deformable Domains,” *45th AIAA Aerospace Sciences Meeting and Exhibit, Reno, Nevada*, January 2007, AIAA-2007-513.
- <sup>10</sup>Visbal, M. R. and Gaitonde, D. V., “On the use of higher-order finite-difference schemes on curvilinear and deforming meshes,” *J. Comput. Phys.*, Vol. 181, No. 1, 2002, pp. 155–185.
- <sup>11</sup>Brown, S. A., “Displacement Extrapolations for CFD+CSM Aeroelastic Analysis,” *35th AIAA Aerospace Sciences Meeting and Exhibit, Reno, Nevada*, January 1997, AIAA-97-1090.
- <sup>12</sup>Bonet, J. and Wood, R. D., *Nonlinear continuum mechanics for finite element analysis*, Cambridge University Press, Cambridge, 1997.
- <sup>13</sup>Cockburn, B. and Shu, C.-W., “The local discontinuous Galerkin method for time-dependent convection-diffusion systems,” *SIAM J. Numer. Anal.*, Vol. 35, No. 6, 1998, pp. 2440–2463 (electronic).
- <sup>14</sup>Peraire, J. and Persson, P.-O., “The Compact Discontinuous Galerkin (CDG) Method for Elliptic Problems,” *in review*, 2006.
- <sup>15</sup>Roe, P. L., “Approximate Riemann solvers, parameter vectors, and difference schemes,” *J. Comput. Phys.*, Vol. 43, No. 2, 1981, pp. 357–372.
- <sup>16</sup>Thomas, P. and Lombard, C., “Geometric conservation law and its application to flow computations on moving grids,” *AIAA Journal*, Vol. 17, 1979.
- <sup>17</sup>Willis, D. J., Israeli, E. R., Persson, P.-O., Drela, M., Peraire, J., Swartz, S. M., and Breuer, K. S., “A Computational Framework for Fluid Structure Interaction in Biologically Inspired Flapping Flight,” *18th AIAA Computational Fluid Dynamics Conference*, June 2007.



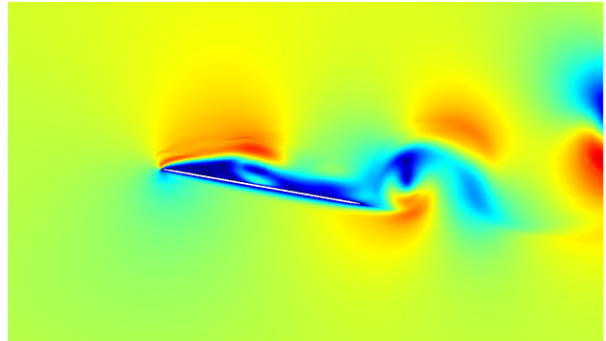
a) Elastic membrane,  $\alpha = 5^\circ$



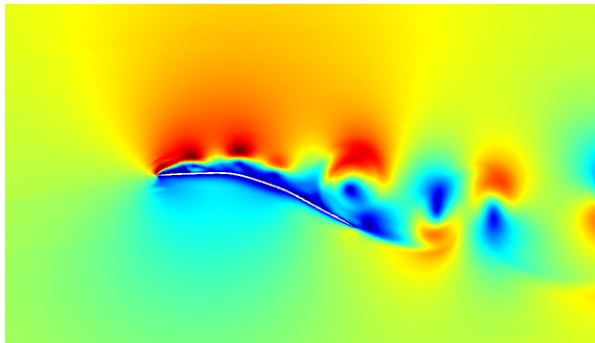
b) Rigid membrane,  $\alpha = 5^\circ$



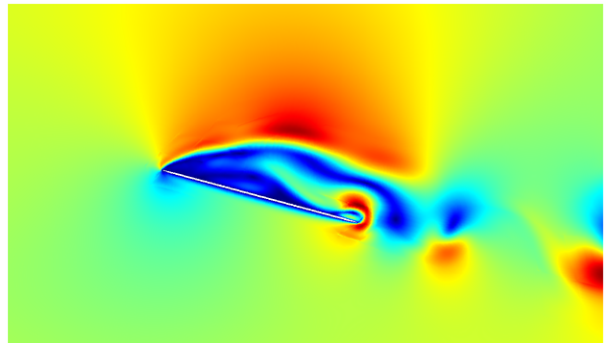
c) Elastic membrane,  $\alpha = 10^\circ$



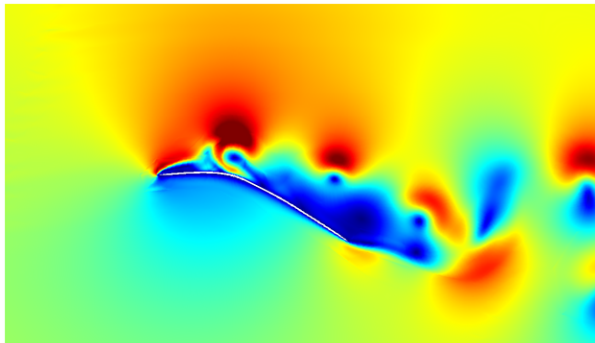
d) Rigid membrane,  $\alpha = 10^\circ$



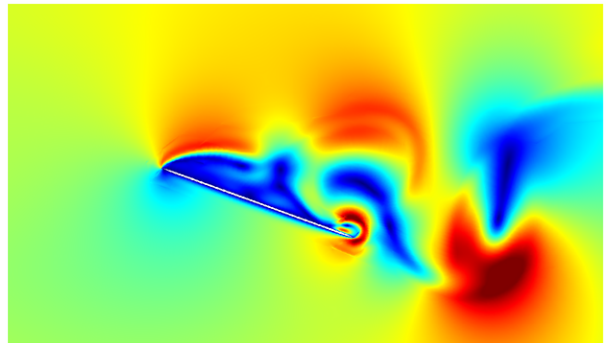
e) Elastic membrane,  $\alpha = 15^\circ$



f) Rigid membrane,  $\alpha = 15^\circ$



g) Elastic membrane,  $\alpha = 20^\circ$



h) Rigid membrane,  $\alpha = 20^\circ$

**Figure 5.** The elastic and rigid membranes with fixed endpoints at time  $t = 10.0$  (Mach number).

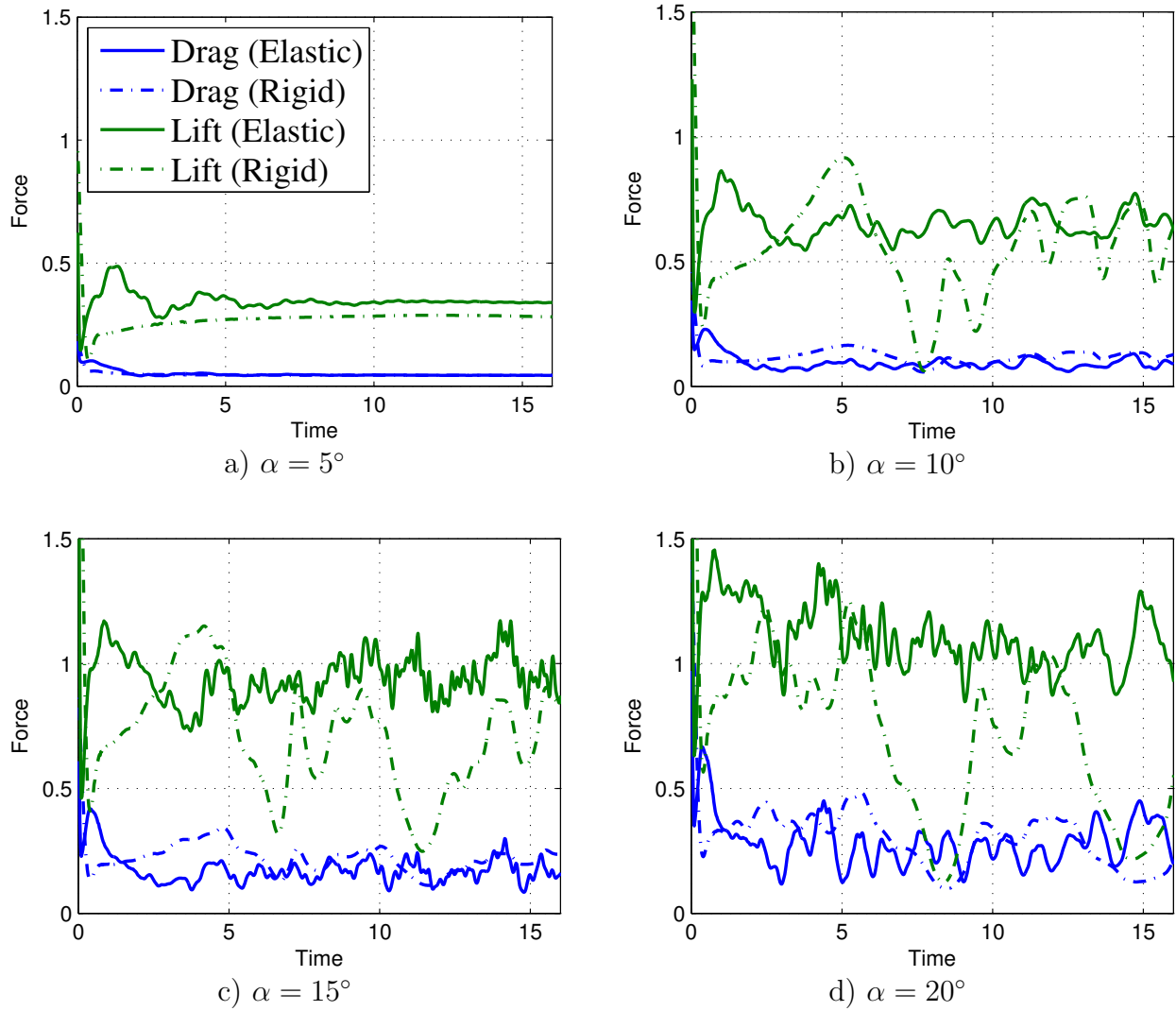


Figure 6. Drag vs. time for the four membrane simulations with fixed endpoints.

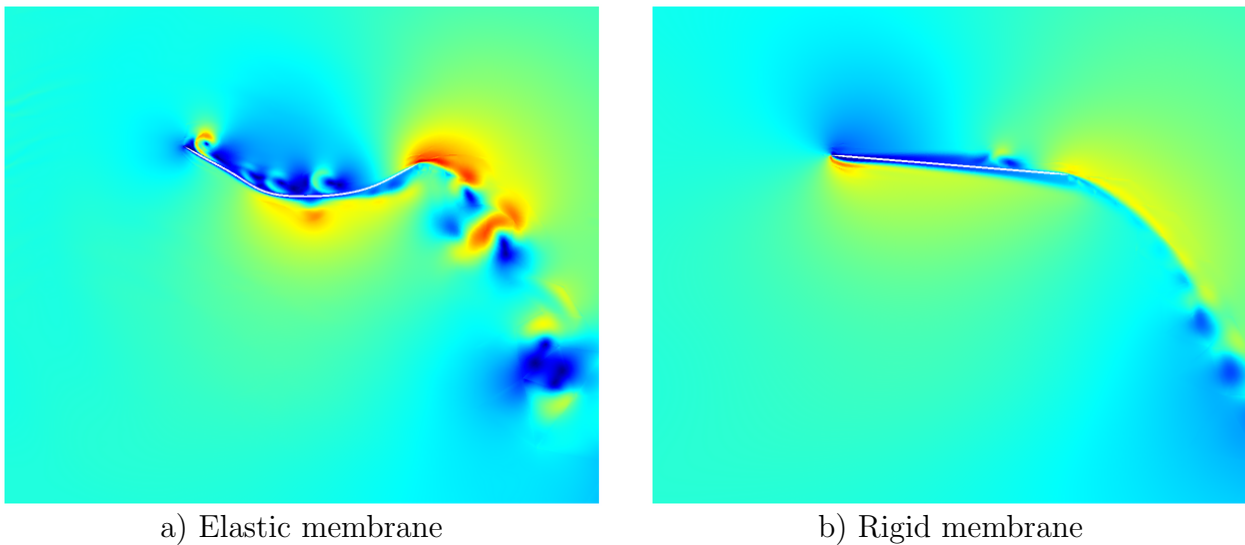


Figure 7. The elastic and rigid membranes with oscillating endpoints at time  $t = 16.125$  (Mach number).